Solitary pulses and periodic wave trains in a bistable FitzHugh-Nagumo model with cross diffusion and cross advection

Evgeny P. Zemskov [1,*] Mikhail A. Tsyganov [2,†] Genrich R. Ivanitsky [2,‡] and Werner Horsthemke [3,§]

[1] *Federal Research Center for Computer Science and Control, Russian Academy of Sciences, Vavilova 40, 119333 Moscow, Russia*

[2] *Institute of Theoretical and Experimental Biophysics, Russian Academy of Sciences, Institutskaya 3, 142290 Pushchino, Moscow Region, Russia*

[3] *Department of Chemistry, Southern Methodist University, Dallas, Texas 75275-0314, USA*

(Received 4 August 2021; accepted 16 November 2021; published 10 January 2022)

We describe analytically, and simulate numerically, traveling waves with oscillatory tails in a bistable, piecewise-linear reaction-diffusion-advection system of the FitzHugh-Nagumo type with linear cross-diffusion and cross-advection terms of opposite signs. We explore the dynamics of two wave types, namely, solitary pulses and their infinite sequences, i.e., periodic wave trains. The effects of cross diffusion and cross advection on wave profiles and speed of propagation are analyzed. For pulses, in the speed diagram splitting of a curve into several branches occurs, corresponding to different waves (wave branching). For wave trains, in the dispersion relation diagram there are oscillatory curves and the discontinuous curve of an isola with two branches. The corresponding wave trains have symmetric or asymmetric profiles. Numerical simulations show that for large values of the period there exist two wave trains, which come closer and closer together and are subject to fusion into one when the value of the period is decreasing. Other types of waves are also briefly discussed.

DOI: 10.1103/PhysRevE.105.014207

I. INTRODUCTION

Spatiotemporal pattern formation in excitable (active) media can be modeled adequately in terms of reaction-diffusion equations. While most theoretical descriptions assume a diagonal diffusion matrix, important applications require the inclusion of off-diagonal terms, i.e., cross-diffusion terms where the diffusion of a species depends on the gradient of another species. Some of the earlier inquiries into this topic are related to the model for interactions between tectonic plates in seismology by Burridge and Knopoff [1–3] and other geological multiphase solids [4–6], the model for chemotaxis by Keller and Segel [7,8], and the equations for the populations of two competing species by Shigesada *et al.* [9]. Over the years, the effects of cross diffusion were explored in various areas, but most prominently in chemistry [10] and in biology and ecology [11,12]. Recent works involve the investigations of the formation of various types of patterns and waves, such as Turing patterns and traveling waves [13–18].

The FitzHugh-Nagumo (FHN) equations [19,20], also known as the Bonhoeffer–van der Pol model [21–23], were originally introduced as a simplification of the Hodgkin–Huxley model [24], which describes the propagation of an action potential along nerve fibers. The FHN model is a system of two reaction-diffusion equations, where the variable $u = u(x,t)$ represents the "activator" or potential variable and the variable $v = v(x,t)$ is the "inhibitor" or recovery variable. The FHN model has been extended to include cross-diffusion effects [25–29]. We consider the specific case that the cross-diffusion terms have opposite signs, i.e., the cross diffusion is attractive-repulsive,

$$\frac{\partial u}{\partial t} = u(1-u)(u-a) - v + D\frac{\partial^2 u}{\partial x^2} + h\frac{\partial^2 v}{\partial x^2}, \tag{1a}$$

$$\frac{\partial v}{\partial t} = \varepsilon(u-v) + D\frac{\partial^2 v}{\partial x^2} - h\frac{\partial^2 u}{\partial x^2}. \tag{1b}$$

The reaction part contains two positive parameters, namely, the excitation threshold a and the ratio of timescales ε. The diffusive part contains two positive constants, D and h, which are the self- and cross-diffusion coefficients, respectively.

Motivated by wave existence arguments for such nonlinear evolution equations, we consider here a generalization of the cross-diffusive FHN model to one with cross advection to explore the interplay of cross diffusion and cross advection on the dynamics of traveling waves. While cross diffusion is well understood in physicochemical systems [10] and ecological systems [11], and its effects in excitable systems have been studied over the last decades (see, for example, [12,25,30]), cross advection, where the motion of one species comes about due to the motion of another species, occurs more rarely and has received less attention. The origins of cross advection in physical, chemical, geophysical, and ecological systems and the motivation for studying the effects of cross advection have been discussed in detail in Ref. [31]. We will not repeat that discussion here and will mention only briefly that though cross advection is rare in physical and chemical systems, it is by no means unknown. Two examples are oxygen-limited

*dr.zemskov@gmail.com
†tsyganov@iteb.ru
‡ivanitsky@iteb.ru
§whorsthe@mail.smu.edu

biodegradation in three-dimensionally heterogeneous aquifers [32] and thermosolutal and binary fluid convection [33]. However, most studies of cross-advection effects are found in the biological, ecological, and population dynamics literature. An example of cross advection is a two-species population, where a parasite moves by convection of a host [12,30]. Cross-advection terms are also found in models for vegetation patterns in arid environments (see, for example, [34,35]), models for moving filaments [36] and directed particle flow [37], descriptions of fully nonlinear strongly coupled competitive systems [38], and models of run-and-tumble dynamics for bacteria [39].

The paper is organized as follows. We describe the model in Sec. II. Section III contains the analytical solutions of the model and a discussion of the propagation behavior for solitary pulses. Wave trains are considered in Sec. IV. We discuss some aspects of the problem and summarize our results in Sec. V

II. MODEL

The FHN model with cross diffusion and cross advection [31] is described by the equations

$$\frac{\partial u}{\partial t} = u(1-u)(u-a) - v + D\frac{\partial^2 u}{\partial x^2} + h\frac{\partial^2 v}{\partial x^2} + j\frac{\partial v}{\partial x}, \quad (2a)$$

$$\frac{\partial v}{\partial t} = \varepsilon(u-v) + D\frac{\partial^2 v}{\partial x^2} - h\frac{\partial^2 u}{\partial x^2} - j\frac{\partial u}{\partial x}. \quad (2b)$$

We consider the specific case that the cross-advective terms have opposite signs, similar to the cross-diffusive terms, and are characterized by one positive constant j. This choice is motivated by previous work [40–42] on the reaction-diffusion system with cross diffusion of opposite signs where we found solitary pulses, periodic wave trains, fronts of complex shapes (pulse-front waves), and bound states of pulses (multipulsons). Our goal here is to assess the additional effect of cross advection on the wave behavior in systems where the cross-diffusion and the cross-advection terms are of the same type, i.e., opposite signs for both.

To solve the system analytically, we consider the case $\varepsilon = 1$, as in previous studies, and apply McKean's piecewise-linear approximation [43–45], where the cubic nonlinearity in the activator equation is replaced by the Heaviside function, $H(u-a)$, so that the FHN model is described by the equations

$$\frac{\partial u}{\partial t} = -u - v + H(u-a) + D\frac{\partial^2 u}{\partial x^2} + h\frac{\partial^2 v}{\partial x^2} + j\frac{\partial v}{\partial x}, \quad (3a)$$

$$\frac{\partial v}{\partial t} = \varepsilon(u-v) + D\frac{\partial^2 v}{\partial x^2} - h\frac{\partial^2 u}{\partial x^2} - j\frac{\partial u}{\partial x}. \quad (3b)$$

We focus our attention here on traveling waves, specifically on solitary pulses and infinite sequences of pulses, i.e., periodic wave trains.

III. SOLITARY PULSES

First we consider traveling wave solutions of the solitary pulse type. The traveling pulses form a homoclinic trajectory in the phase plane (u, v) and in the piecewise-linear model

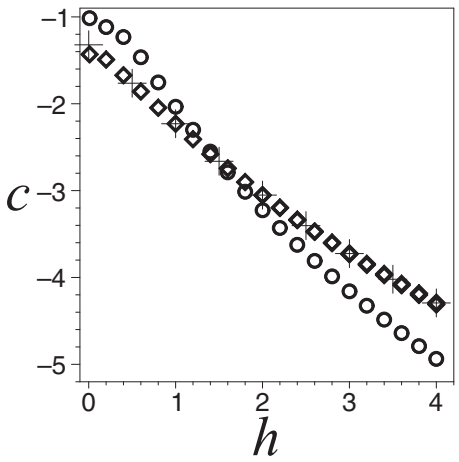

FIG. 1. Speed of the pulse waves as a function of the cross-diffusion coefficient, $c = c(h)$. The values of the excitation threshold, the ratio of the timescales, and the self-diffusion and cross-advection coefficients are fixed at $a = 1/4$, $\varepsilon = 1$, $D = 1$, and $j = 1$, respectively. Results of analytical calculations are marked by circles (narrow wave) and diamonds (wide wave), while numerical simulations are marked by crosses.

consist of three parts that are fitted together using a specific matching procedure. The three parts of the pulse solutions are given by [40]

$$u_1(\xi) = e^{k_+\xi}[A_{11}\cos(l_-\xi) + A_{13}\sin(l_-\xi)], \quad (4a)$$

$$u_2(\xi) = e^{k_+\xi}[A_{21}\cos(l_-\xi) + A_{23}\sin(l_-\xi)] + e^{k_-\xi}[A_{22}\cos(l_+\xi) + A_{24}\sin(l_+\xi)] + 1/2, \quad (4b)$$

$$u_3(\xi) = e^{k_-\xi}[A_{32}\cos(l_+\xi) + A_{34}\sin(l_+\xi)], \quad (4c)$$

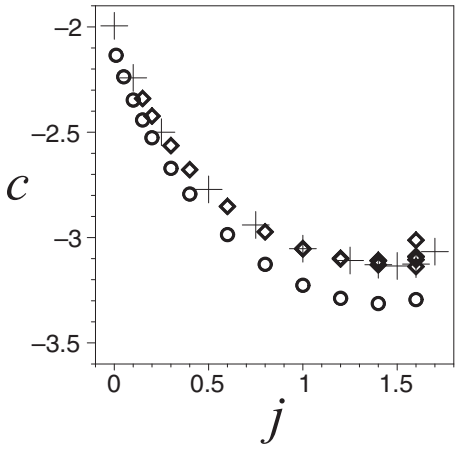

FIG. 2. Speed of the pulse waves as a function of the cross-advection coefficient, $c = c(j)$. The values of the excitation threshold, the ratio of the timescales, and the self- and cross-diffusion coefficients are fixed at $a = 1/4$, $\varepsilon = 1$, $D = 1$, and $h = 2$, respectively. Results of analytical calculations are marked by circles (narrow wave) and diamonds (wide wave), while numerical simulations are marked by crosses.

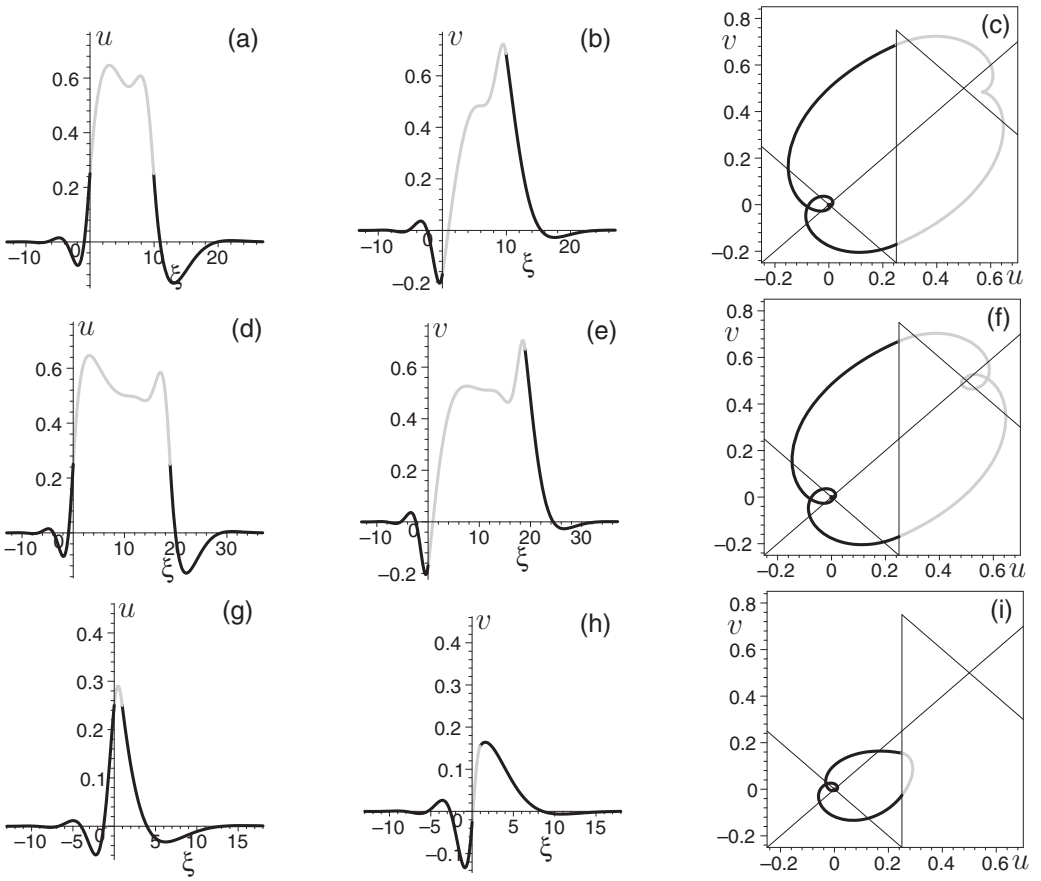

FIG. 3. Solitary pulse waves for weak cross advection. Profiles for the activator $u = u(\xi)$ (a,d,g), for the inhibitor $v = v(\xi)$ (b,e,h), and in the (u, v)-phase plane (bold lines) (c,f,i). The waves propagate with the speed $c \approx -3.0525$ (a,b,c), $c \approx -3.0535$ (d,e,f), and $c \approx -3.2267$ (g,h,i). The cross-advection coefficient is fixed at $j = 1$. The excitation threshold, the ratio of the timescales, and the self- and cross-diffusion coefficients are fixed at $a = 1/4$, $\varepsilon = 1$, $D = 1$, and $h = 2$, respectively. The middle parts, u_2 and v_2, of the pulses are indicated by the gray color. The nullclines $f(u, v) = -u - v + H(u - a) = 0$ and $g(u, v) = u - v = 0$ are marked by thin lines in panels (c,f,i).

for the activator variable, and

$$v_1(\xi) = e^{k_+\xi}[B_{11}\cos(l_-\xi) + B_{13}\sin(l_-\xi)], \tag{5a}$$

$$v_2(\xi) = e^{k_+\xi}[B_{21}\cos(l_-\xi) + B_{23}\sin(l_-\xi)] + e^{k_-\xi}[B_{22}\cos(l_+\xi) + B_{24}\sin(l_+\xi)] + 1/2, \tag{5b}$$

$$v_3(\xi) = e^{k_-\xi}[B_{32}\cos(l_+\xi) + B_{34}\sin(l_+\xi)], \tag{5c}$$

for the inhibitor variable.

Here the notations $k_\pm$ and $l_\pm$ stand for $k_\pm = \pm y - p$ and $l_\pm = z \pm q$, respectively, where [31]

$$p = \frac{cD + jh}{2(D^2 + h^2)}, \tag{6a}$$

$$q = \frac{ch - jD}{2(D^2 + h^2)}, \tag{6b}$$

$$b = p^2 - q^2 + \frac{D + h}{D^2 + h^2}, \tag{6c}$$

$$d = 2pq - \frac{D - h}{D^2 + h^2}, \tag{6d}$$

$$y = \sqrt{(\sqrt{b^2 + d^2} + b)/2}, \tag{6e}$$

$$z = \sqrt{(\sqrt{b^2 + d^2} - b)/2}. \tag{6f}$$

The integration constants B are expressed as

$$B_{1,3} = -\frac{1}{\gamma_1^2 + \delta_1^2}[(\alpha_1\gamma_1 + \beta_1\delta_1)A_{1,3} \mp (\alpha_1\delta_1 - \beta_1\gamma_1)A_{3,1}], \tag{7a}$$

$$B_{2,4} = -\frac{1}{\gamma_2^2 + \delta_2^2}[(\alpha_2\gamma_2 + \beta_2\delta_2)A_{2,4} \mp (\alpha_2\delta_2 - \beta_2\gamma_2)A_{4,2}], \tag{7b}$$

with

$$\begin{aligned} \alpha_1 &= D(k_+^2 - l_-^2) + ck_+ - 1, \quad \beta_1 = l_-(2Dk_+ + c), \\ \gamma_1 &= h(k_+^2 - l_-^2) + jk_+ - 1, \quad \delta_1 = l_-(2hk_+ + j), \\ \alpha_2 &= D(k_-^2 - l_+^2) + ck_- - 1, \quad \beta_2 = l_+(2Dk_- + c), \\ \gamma_2 &= h(k_-^2 - l_+^2) + jk_- - 1, \quad \delta_2 = l_+(2hk_- + j). \end{aligned} \tag{8}$$

The dynamics of the pulse waves is illustrated by the speed diagrams in Figs. 1 and 2. The first diagram displays the behavior of the wave speed c as a function of the cross-diffusion coefficient h, while the second one displays the behavior as a function of the cross-advection coefficient j with all other

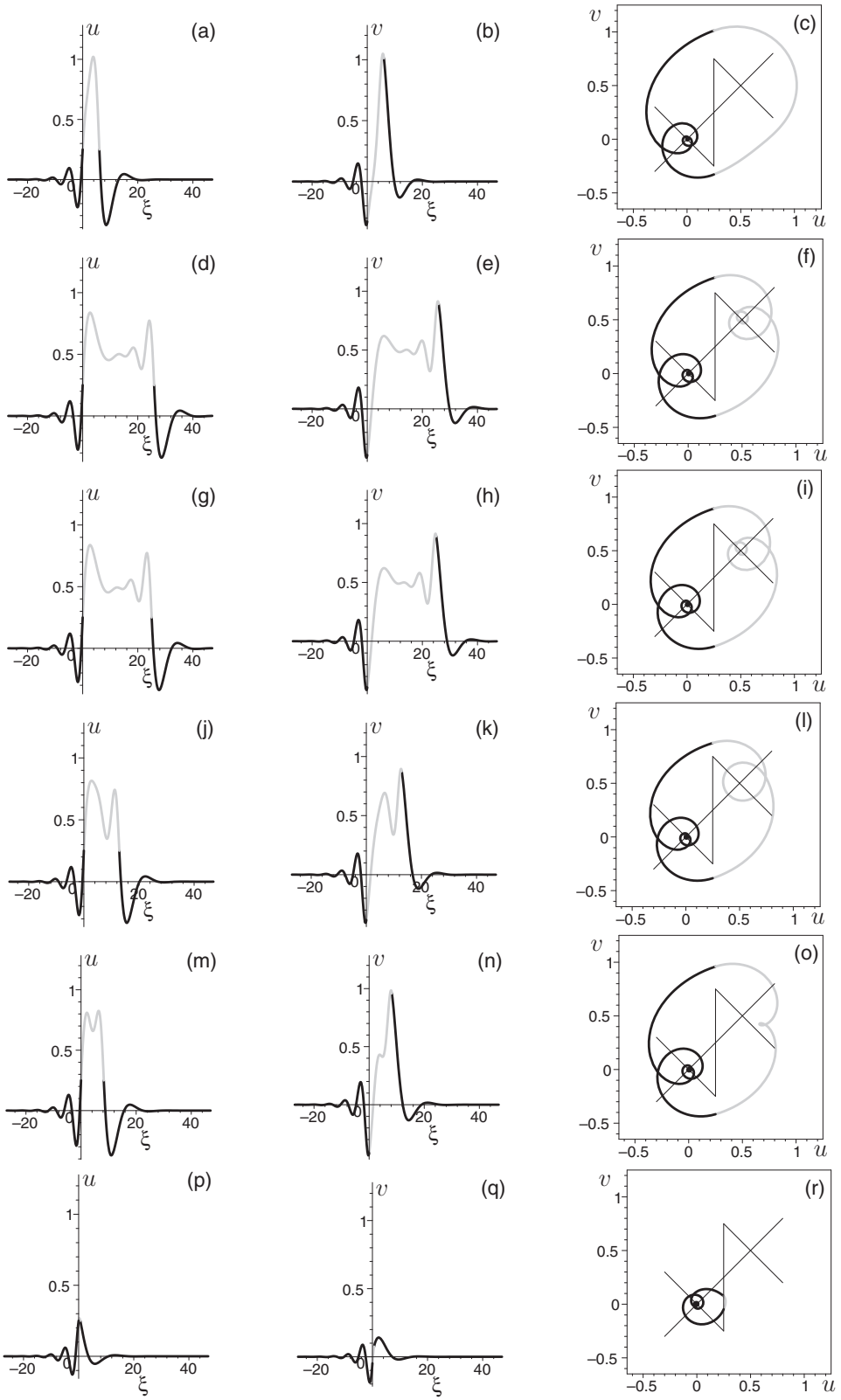

FIG. 4. Solitary pulse waves for strong cross advection. Profiles for the activator $u = u(\xi)$ (a,d,g,j,m,p), for the inhibitor $v = v(\xi)$ (b,e,h,k,n,q), and in the (u, v)-phase plane (bold lines) (c,f,i,l,o,r). The waves propagate with the speed $c \approx -3.0123$ (a,b,c), $c \approx -3.0903$ (d,e,f), $c \approx -3.0906$ (g,h,i), $c \approx -3.1051$ (j,k,l), $c \approx -3.1378$ (m,n,o), and $c \approx -3.2947$ (p,q,r). The cross-advection coefficient is fixed at $j = 1.6$; all other parameters are the same as in Fig. 3.

model parameters fixed. The plot of c as a function of h shows that the speed of the pulses increases (in the absolute value) as the cross-diffusion coefficient increases. The range of the cross-diffusion coefficient shown, $h \in [0.01, 4]$, splits up into two intervals, namely, [0.01,1.4] and [1.6,4]. (No points were calculated in between the two intervals.) In the first interval, two pulses exist, the narrow wave (marked by circles in the figure) and the wide one (marked by diamonds). The narrow wave is slow whereas the wide one is fast. The situation changes substantially in the second interval, where (i) three waves appear, one narrow wave and two wide waves, and (ii) the points in the diagram corresponding to the narrow and wide waves change places with each other, so that now the narrow wave (circles) is fast while the two wide waves (diamonds) are slow. The two wide waves differ by their width but have almost the same speed values, so that they are not visually distinguishable in the speed diagram. The related wave profiles for the activator u and inhibitor v variables and the (u, v)-phase planes are plotted in Figs. 3(a,b,c) and 3(d,e,f) for the two wide waves and in Figs. 3(g,h,i) for the narrow wave.

The second speed diagram, Fig. 2, shows the dependence of c on j, which displays a more complex behavior. When the cross-advection coefficient j is small, there exists only one narrow wave. Then the wide wave appears as j increases. At $j = 1$, already two wide waves occur, and they are visually distinguishable at $j = 1.4$. The appearance of additional waves, the *wave branching*, evolves rapidly, and there exist six pulses at $j = 1.6$. With further increases of $j > 1.7$, the oscillations in the pulse profiles grow and the wave shape exhibits a pattern, which is an extension of the pulse solutions that intersect $a = 1/4$ many times. In other words, such a pulse must consist of more than three parts, and this construction can not be described by the approach used here. Consequently, we restrict our consideration to $j = 1.6$ and plot the associated six waves in Fig. 4. We observe two waves, which are almost the same, in Figs. 4(d,e,f) and 4(g,h,i). These waves differ slightly in their widths (25.92 and 25.036) and in their speed values (-3.0903 and -3.0906). Note that this wave branching does not represent some kind of self-replication process of the pulses. We emphasize that this phenomenon differs substantially from the wave splitting observed in Ref. [46], where two or more waves appear together simultaneously in the medium. In our case there is only one pulse in the medium at each instant of time; the branching occurs in parameter space, i.e., in the speed diagram.

The appearance of multiple pulse solutions, the multiwave regime, requires a more detailed analysis of the stability of these waves. To evaluate the stability of the solutions, we have obtained the solutions numerically from the PDEs of the basic model (3). The results of numerical simulations for the propagation of the pulse waves are shown in the speed diagrams in Figs. 1 and 2 marked by crosses. They reveal that only one pulse solution, marked by diamonds in both figures, is realized, i.e., is stable. The numerical simulations show that the wave from Figs. 4(m,n,o) is stable. The numerical result for speed is $c = -3.126$ and the analytical result is $c = -3.1378$. During the numerical simulations of the process of wave formation, several waves with different speed values appear, but only the wave with the above speed survives, indicating that the other five waves are unstable.

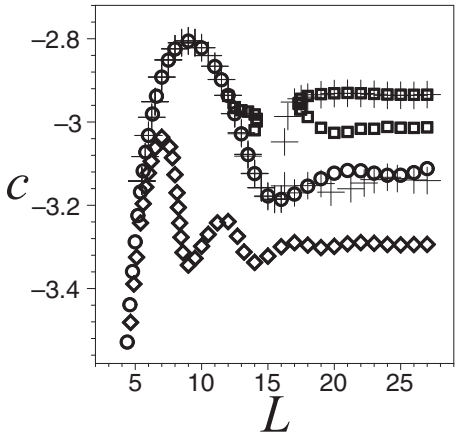

FIG. 5. Speed of the periodic wave train as a function of the period (dispersion relation), $c = c(L)$, for strong cross advection, $j = 1.6$; all other parameters are the same as in Fig. 3. Wave trains with symmetric profiles are marked by circles, while asymmetric waves are marked by diamonds and squares (analytical calculations). Results of numerical simulations are marked by crosses.

IV. PERIODIC WAVE TRAINS

Next we consider infinite sequences of pulses, i.e., periodic wave trains. The wave trains form a closed smooth trajectory in the (u, v)-phase plane and in the piecewise-linear model consist of two parts that are matched together. The two parts of the wave train solutions are given by [40]

$$u_1(\xi) = e^{k_+\xi}[A_{11}\cos(l_-\xi) + A_{13}\sin(l_-\xi)] + e^{k_-\xi}[A_{12}\cos(l_+\xi) + A_{14}\sin(l_+\xi)], \tag{9a}$$

$$u_2(\xi) = e^{k_+\xi}[A_{21}\cos(l_-\xi) + A_{23}\sin(l_-\xi)] + e^{k_-\xi}[A_{22}\cos(l_+\xi) + A_{24}\sin(l_+\xi)] + 1/2 \tag{9b}$$

for the activator variable, and

$$v_1(\xi) = e^{k_+\xi}[B_{11}\cos(l_-\xi) + B_{13}\sin(l_-\xi)] + e^{k_-\xi}[B_{12}\cos(l_+\xi) + B_{14}\sin(l_+\xi)], \tag{10a}$$

$$v_2(\xi) = e^{k_+\xi}[B_{21}\cos(l_-\xi) + B_{23}\sin(l_-\xi)] + e^{k_-\xi}[B_{22}\cos(l_+\xi) + B_{24}\sin(l_+\xi)] + 1/2 \tag{10b}$$

for the inhibitor variable.

The dynamics of the wave trains is illustrated by the dispersion relation, which reflects the dependence of the speed c of the wave train on the period of the wave train L. The dispersion relation diagram is shown in Fig. 5 when the cross-advection effect is strong, as in Fig. 4 for the solitary pulses. The diagram shows that there exist three types of curves, indicated by circles, diamonds, and squares in the figure. As expected, for wave trains with oscillatory tails the dispersion relation shows oscillatory behavior, the circles and diamonds in the figure. However, there is an unexpected feature, namely, an isola, i.e., a discontinuous curve with two branches, represented by the squares in figure. The wave trains corresponding to the circles in the diagram have a symmetric profile, where the inner matching point, which is inside of the period, is in the middle. These wave trains are shown in Fig. 6 for increasing the period L; all other parameters are fixed.

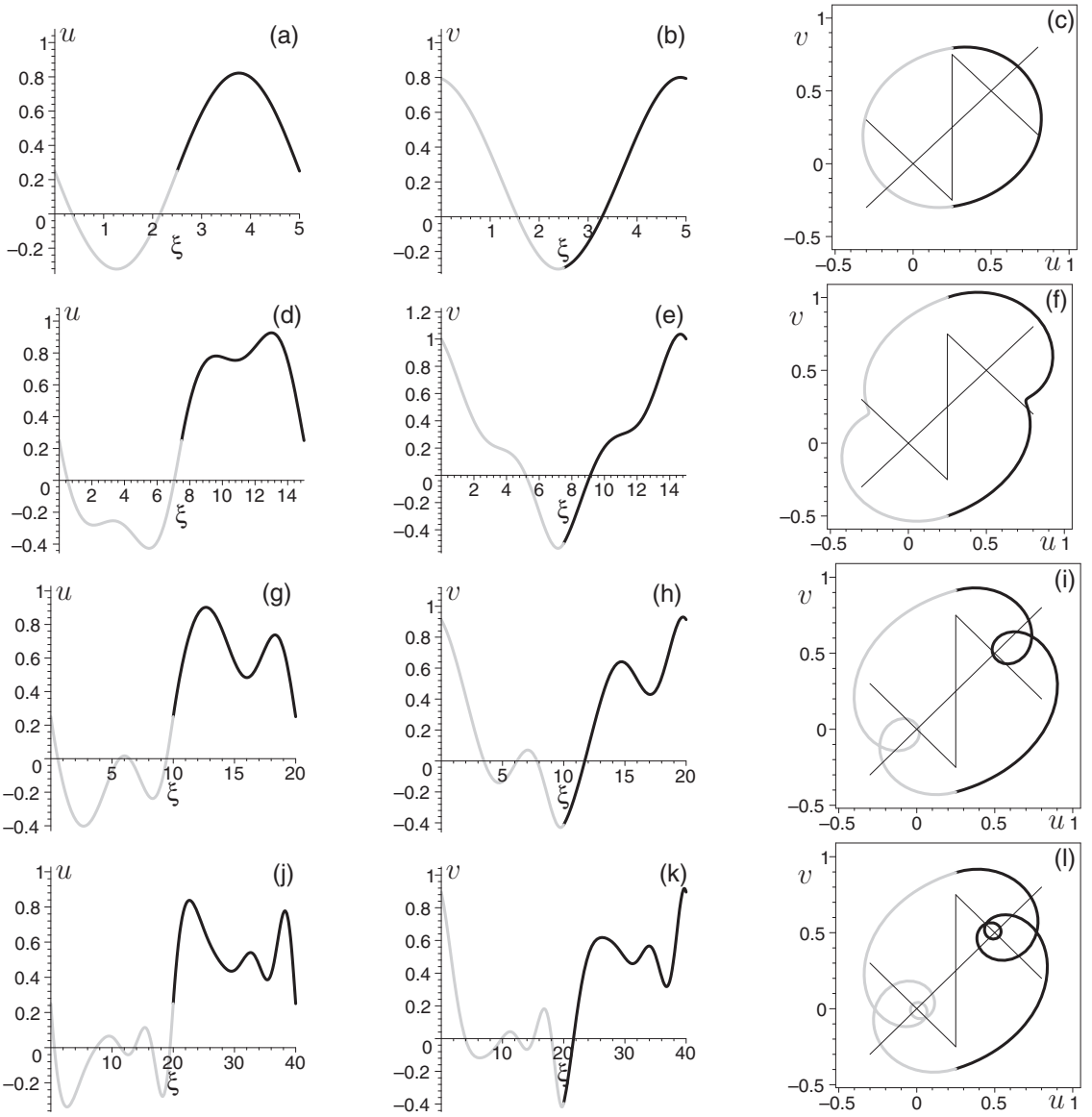

FIG. 6. Periodic wave trains with symmetric profiles (corresponding to circles in Fig. 5; one period is shown) for the activator $u = u(\xi)$ (a,d,g,j), for the inhibitor $v = v(\xi)$ (b,e,h,k), and in the (u, v)-phase plane (bold lines) (c,f,i,l). Panels (a,b,c) correspond to the period $L = 5$, where the calculated speed is $c \approx -3.2879$, panels (d,e,f) to $L = 15$, where the calculated speed is $c \approx -3.1777$, panels (g,h,i) to $L = 20$, where the calculated speed is $c \approx -3.1230$, and panels (j,k,l) to $L = 40$, where the calculated speed is $c \approx -3.0910$. The cross-advection coefficient is fixed at $j = 1.6$; all other parameters are the same as in Fig. 3. The first parts, u_1 and v_1, of the wave trains are indicated by the gray color.

The wave trains corresponding to the diamonds and squares in the diagram have asymmetric profiles and are shown in Figs. 7 and 8, respectively. For each asymmetric case there exist two wave trains: one wave train with the inner matching point ξ_0 placed in the $(0, L/2)$ interval and one wave train with $\xi_0 \in (L/2, L)$. Both of these wave trains have the same value of the propagation speed and have profiles that are rearranged with respect to one another when the inner matching point changes its location from $(0, L/2)$ to $(L/2, L)$. Therefore we show in Figs. 7 and 8 only one wave train, namely, the one with $\xi_0 \in (0, L/2)$.

The asymmetric wave trains corresponding to the diamonds and the squares differ in size: the "diamond" wave train is small and localized near the second fixed point at $u = v = 1/2$ in the (u, v)-phase plane, Figs. 7(c,f,i,l). This is the case because the inner matching point is placed in the $(0, L/2)$ interval. The asymmetric wave train with $\xi_0 \in (L/2, L)$, which is not shown, is localized near the first fixed point at $u = v = 0$. The "square" wave train is large and visits the vicinity of both fixed points, Figs. 8(c,f,i,l), but inner loops in the (u, v)-phase plane appear near the second fixed point at $u = v = 1/2$ due to the choice of ξ_0, as for the "diamond" wave train. The "square" wave trains are shown in Fig. 8 mostly for the slow wave, in terms of the absolute value of the speed, corresponding to the upper branch of the speed curve in Fig. 5, with the exception of Figs. 8(j,k,l), where the "square" wave train corresponding to the lower branch is displayed for comparison.

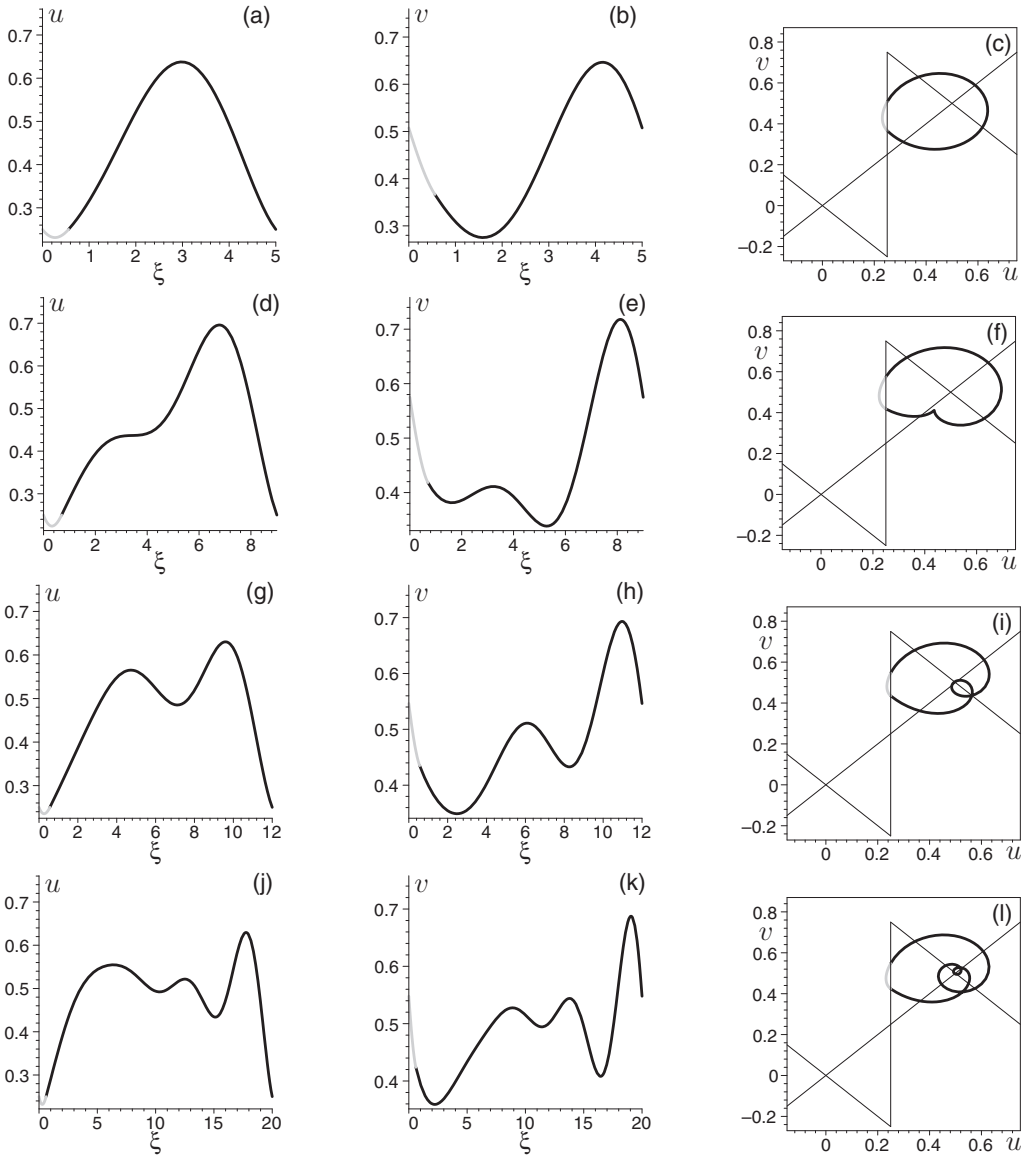

FIG. 7. Periodic wave trains with asymmetric profiles (corresponding to diamonds in Fig. 5; one period is shown) for the activator $u = u(\xi)$ (a,d,g,j), for the inhibitor $v = v(\xi)$ (b,e,h,k), and in the (u, v)-phase plane (bold lines) (c,f,i,l). Panels (a,b,c) correspond to the period $L = 5$, where the calculated speed is $c \approx -3.3561$, panels (d,e,f) to $L = 9$, where the calculated speed is $c \approx -3.3438$, panels (g,h,i) to $L = 12$, where the calculated speed is $c \approx -3.2393$, and panels (j,k,l) to $L = 20$, where the calculated speed is $c \approx -3.2988$. The cross-advection coefficient is fixed at $j = 1.6$; all other parameters are the same as in Fig. 3. The first parts, u_1 and v_1, of the wave trains are indicated by the gray color.

All wave trains are calculated for characteristic values of the period where the shape of the wave train profile changes significantly. The symmetric wave train at $L = 5$ has simple sinelike profiles, Figs. 6(a,b), and a one-loop shape in the (u, v)-phase plane, Fig. 6(c). Then at $L = 15$, the profiles become deformed, Figs. 6(d,e), so that there is a pair of cusps in the (u, v)-phase plane, Fig. 6(f). When the period is increased further, the oscillations in the profiles become more pronounced, Figs. 6(g,h), and the two cusps transform into two inner loops at $L = 20$, Fig. 6(i). Such a process of inner loop formation repeats again; at $L = 40$, Fig. 6(l), two "new" inner loops appear inside the "old" inner loops. We did not perform calculations for $L > 40$, due to the limitations of our two-part construction for the wave train. When the period is sufficiently large, the oscillations in the profiles become too strong and intersect the line corresponding to the inner matching point, so that a construction with more than two parts needs to be considered. Nevertheless, we expect that the process of inner loop formation occurs over and over again as the period is increased. The scenario of the profile oscillation growth with the loop formation in the phase plane remains the same also for both asymmetric wave trains pictured in Figs. 7 and 8, except for a single inner loop and for different values of the period.

The results of numerical simulations for the propagation of the wave trains are also shown in the dispersion relation diagram in Fig. 5, marked by crosses. The calculations were started at a value of $L = 34$. The period was then decreased, down to $L = 5.5$. The numerical results show that for large values of the period there exist two wave trains, which were

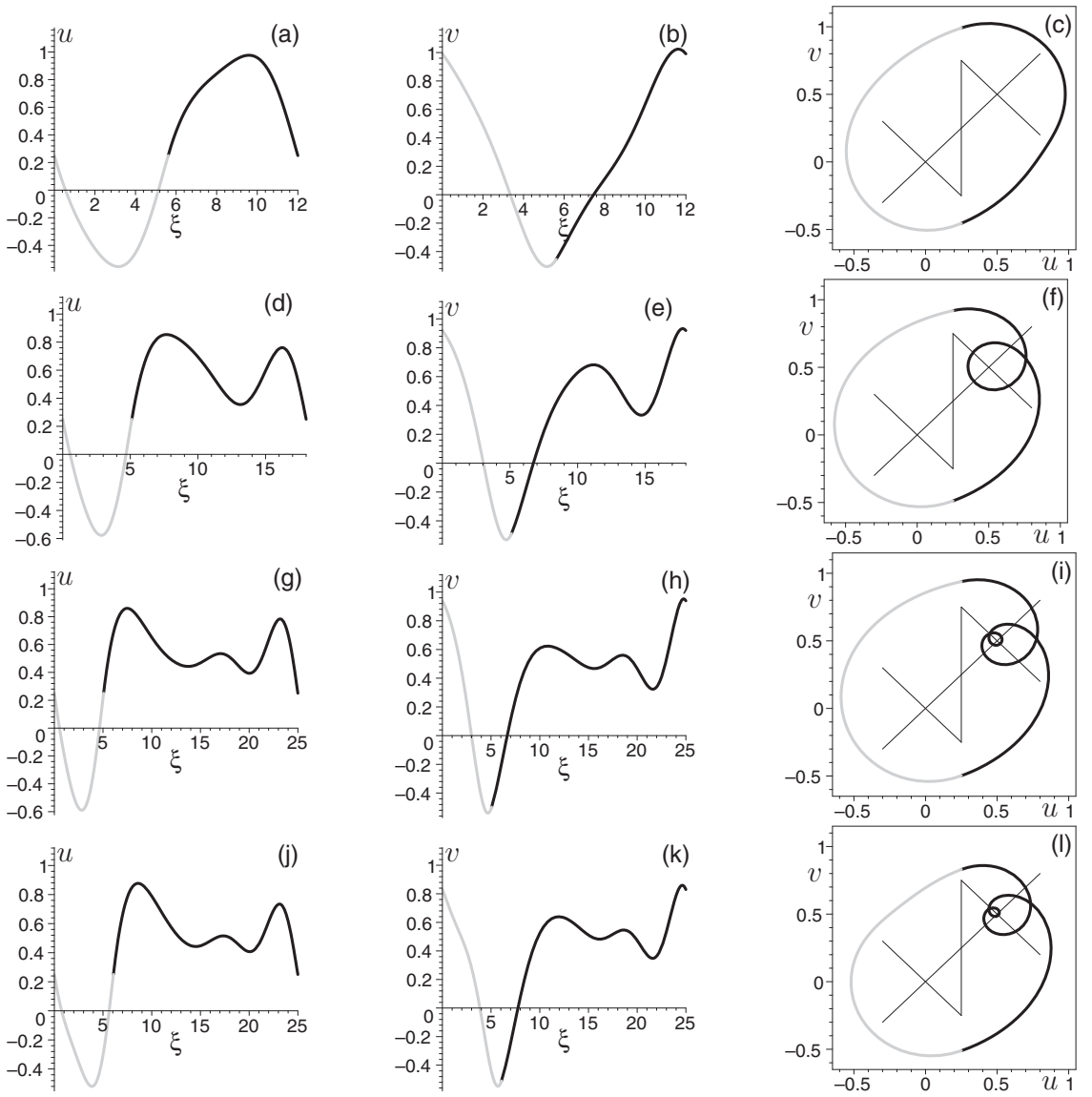

FIG. 8. Periodic wave trains with asymmetric profiles (corresponding to squares in Fig. 5; one period is shown) for the activator $u = u(\xi)$ (a,d,g,j), for the inhibitor $v = v(\xi)$ (b,e,h,k), and in the (u, v)-phase plane (bold lines) (c,f,i,l). Panels (a,b,c) correspond to the period $L = 12$, where the calculated speed is $c \approx -2.9375$, panels (d,e,f) to $L = 18$, where the calculated speed is $c \approx -2.9374$, and panels (g,h,i) and (j,k,l) to $L = 25$, where the calculated speeds are $c \approx -2.9346$ (g,h,i) and $c \approx -3.0138$ (j,k,l). The cross-advection coefficient is fixed at $j = 1.6$; all other parameters are the same as in Fig. 3. The first parts, u_1 and v_1, of the wave trains are indicated by the gray color.

obtained using different initial perturbations in the medium. The data for the first wave train fit well the upper branch of the "square" curve for $L \geqslant 17.5$ in the figure, while the data for the second wave train correspond to the "circle" curve with small deviations from the analytical results at $L \approx 20, \ldots, 22, 27$. When the value of the period continues to decrease, these two wave trains come closer and closer together and are subject to fusion into one wave at $L \approx 16$, so that for small values of the period, $L < 16$, only the wave train with a symmetric profile (circles) is realized.

V. CONCLUSIONS

Fronts, pulses, and wave trains belong to the three basic nonlinear waves that are quintessential for excitable systems like the FHN model. Previous studies showed that the inclusion of cross-diffusion effects in the FHN model leads to new features, such as the existence of fronts with complex shape, the pulse-front waves [41], as well as bound states of pulses, finite pulse trains or multipulsons [42] with specific behavior of propagation, namely, solitonic-type interaction upon collision [30]. We expected therefore that the inclusion of cross advection in addition to cross diffusion would give rise to new spatiotemporal behavior. We discussed briefly in Sec. I, referring to Ref. [31], the motivation for including cross-advection terms and provided several applications where such terms are encountered. In our previous work [31] we focused on fronts in the FHN systems with cross advection. The other two types of basic traveling waves in reaction-diffusion systems are solitary pulses

and their infinite sequences (periodic wave trains). Solitary pulses and the periodic wave trains differ crucially from fronts and require a separate treatment, performed in this work.

We have considered here such an extension of the FHN model with cross advection and obtained the wave solutions for pulses and wave trains. The solutions for fronts were obtained earlier in Ref. [31]. Specifically, we have studied the bistable piecewise-linear FitzHugh-Nagumo model with linear cross-diffusion and cross-advection terms with opposite signs and obtained the traveling wave solutions and the speed diagrams for solitary pulses and for infinite sequences of pulses, i.e., periodic wave trains. Fronts, pulses, and wave trains are also observed in the original bistable FHN model with cross diffusion [40,47], but we note that the latter two types of waves show more complex dynamics in the model studied here compared with the FHN model with cross diffusion only. The speed versus cross-advection coefficient diagram for pulses exhibits wave branching where a single curve splits up into many branches, corresponding to waves with different profiles and speed values. The dispersion relation for wave trains is anomalous and contains oscillatory curves, as well as an isola, a discontinuous curve with two branches. Numerical simulations show that for large values of the period there exist two wave trains, which come closer and closer together are finally subject to fusion into one wave train as the value of the period is decreased. Our results reveal that the inclusion of cross advection does indeed have nontrivial effects which change qualitatively the spatiotemporal dynamics of reaction-diffusion systems with cross diffusion.

Here we have described solitary pulses and the periodic wave trains in the piecewise-linear FHN reaction-diffusion system with cross diffusion and cross advection, each of opposite sign. We plan to investigate other types of waves in this system elsewhere. A second direction for future works concerns the stability analysis of different solutions.

[1] R. Burridge and L. Knopoff, Model and theoretical seismicity, Bull. Seismol. Soc. Am. **57**, 341 (1967).

[2] J. H. E. Cartwright, E. Hernández-García, and O. Piro, Burridge-Knopoff Models as Elastic Excitable Media, Phys. Rev. Lett. **79**, 527 (1997).

[3] J. H. E. Cartwright, V. M. Eguíluz, E. Hernández-García, and O. Piro, Dynamics of elastic excitable media, Int. J. Bif. Chaos **09**, 2197 (1999).

[4] K. Regenauer-Lieb, M. Hu, C. Schrank, X. Chen, S. P. Clavijo, U. Kelka, A. Karrech, O. Gaede, T. Blach, H. Roshan, and A. B. Jacquey, Cross-diffusion waves resulting from multiscale, multi-physics instabilities: Theory, Solid Earth **12**, 869 (2021).

[5] K. Regenauer-Lieb, M. Hu, C. Schrank, X. Chen, S. P. Clavijo, U. Kelka, A. Karrech, O. Gaede, T. Blach, H. Roshan, A. B. Jacquey, and P. Szymczak, Cross-diffusion waves as a trigger for multiscale, multiphysics instabilities: Application to earthquakes, Solid Earth **12**, 1829 (2021).

[6] M. Hu, C. Schrank, and K. Regenauer-Lieb, Cross-diffusion waves in hydro-poro-mechanics, J. Mech. Phys. Solids **135**, 103632 (2020).

[7] E. F. Keller and L. A. Segel, Model for chemotaxis, J. Theor. Biol. **30**, 225 (1971).

[8] G. R. Ivanitskii, A. B. Medvinskii, and M. A. Tsyganov, From disorder to order as applied to the movement of microorganisms, Sov. Phys. Uspekhi **34**, 289 (1991).

[9] N. Shigesada, K. Kawasaki, and E. Teramoto, Spatial segregation of interacting species, J. Theor. Biol. **79**, 83 (1979).

[10] V. K. Vanag and I. R. Epstein, Cross-diffusion and pattern formation in reaction–diffusion systems, Phys. Chem. Chem. Phys. **11**, 897 (2009).

[11] A. Okubo and S. A. Levin, *Diffusion and Ecological Problems* (Springer-Verlag, New York, 2001).

[12] M. A. Tsyganov, V. N. Biktashev, J. Brindley, A. V. Holden, and G. R. Ivanitskii, Waves in systems with cross-diffusion as a new class of nonlinear waves, Phys. Usp. **50**, 263 (2007).

[13] N. Kumar and W. Horsthemke, Effects of cross diffusion on Turing bifurcations in two-species reaction-transport systems, Phys. Rev. E **83**, 036105 (2011).

[14] G. Gambino, M. C. Lombardo, and M. Sammartino, Turing instability and traveling fronts for a nonlinear reaction–diffusion system with cross-diffusion, Math. Comput. Simul. **82**, 1112 (2012).

[15] G. Gambino, M. C. Lombardo, and M. Sammartino, Cross-diffusion-induced subharmonic spatial resonances in a predator-prey system, Phys. Rev. E **97**, 012220 (2018).

[16] G. Gambino, M. C. Lombardo, G. Rubino, and M. Sammartino, Pattern selection in the 2D FitzHugh–Nagumo model, Ric. Mat. **68**, 535 (2019).

[17] C. Currò and G. Valenti, Pattern formation in hyperbolic models with cross-diffusion: Theory and applications, Physica D **418**, 132846 (2021).

[18] M. Banerjee, S. Ghoraj, and N. Mukherjee, Study of cross-diffusion induced Turing patterns in a ratio-dependent prey-predator model via amplitude equations, Appl. Math. Model. **55**, 383 (2018).

[19] R. FitzHugh, Impulses and physiological states in theoretical models of nerve membrane, Biophys. J. **1**, 445 (1961).

[20] J. Nagumo, S. Arimoto, and S. Yoshizawa, An active pulse transmission line simulating nerve axon, Proc. IRE **50**, 2061 (1962).

[21] B. van der Pol, On relaxation-oscillations, Philos. Mag. **2**, 978 (1926).

[22] K. F. Bonhoeffer, Über die Aktivierung von Passivem Eisen in Salpetersäure, Z. Elektrochem. **47**, 147 (1941).

[23] K. F. Bonhoeffer, Activation of passive iron as a model for the excitation of nerve, J. Gen. Physiol. **32**, 69 (1948).

[24] A. L. Hodgkin and A. F. Huxley, A quantitative description of membrane current and its application to conduction and excitation in nerve, J. Physiol. **117**, 500 (1952).

[25] V. N. Biktashev and M. A. Tsyganov, Solitary waves in excitable systems with cross-diffusion, Proc. R. Soc. London, Ser. A **461**, 3711 (2005).

[26] F. Berezovskaya, E. Camacho, S. Wirkus, and G. Karev, "Traveling wave" solutions of FitzHugh model with cross-diffusion, Math. Biosci. Eng. **5**, 239 (2008).

[27] F. Berezovskaya, Traveling waves impulses of FitzHugh model with diffusion and cross-diffusion, in *Mathematical Sciences with Multidisciplinary Applications*, edited by B. Toni, Springer Proceedings in Mathematics & Statistics Vol. 157 (Springer, Cham, 2016), pp. 1–20.

[28] V. N. Biktashev and M. A. Tsyganov, Envelope Quasisolitons in Dissipative Systems with Cross-Diffusion, Phys. Rev. Lett. **107**, 134101 (2011).

[29] M. A. Tsyganov and V. N. Biktashev, Classification of wave regimes in excitable systems with linear cross diffusion, Phys. Rev. E **90**, 062912 (2014).

[30] M. A. Tsyganov, J. Brindley, A. V. Holden, and V. N. Biktashev, Quasisoliton Interaction of Pursuit-Evasion Waves in a Predator-Prey System, Phys. Rev. Lett. **91**, 218102 (2003).

[31] E. P. Zemskov, K. Kassner, M. A. Tsyganov, and M. J. B. Hauser, Wavy fronts in reaction-diffusion systems with cross advection, Eur. Phys. J. B **72**, 457 (2009).

[32] F. Miralles-Wilhelm, L. W. Gelhar, and V. Kapoor, Stochastic analysis of oxygen-limited biodegradation in three-dimensionally heterogeneous aquifers, Water Resour. Res. **33**, 1251 (1997).

[33] L. S. Tuckerman, Thermosolutal and binary fluid convection as a 2×2 matrix problem, Physica D **156**, 325 (2001).

[34] J. von Hardenberg, E. Meron, M. Shachak, and Y. Zarmi, Diversity of Vegetation Patterns and Desertification, Phys. Rev. Lett. **87**, 198101 (2001).

[35] X. Wang and G. Zhang, The influence of infiltration feedback on the characteristic of banded vegetation pattern on hillsides of semiarid area, PLoS One **14**, e0205715 (2019).

[36] H. Freistühler, J. Fuhrmann, and A. Stevens, Traveling waves emerging in a diffusive moving filament system, in *Managing Complexity, Reducing Perplexity*, edited by M. Delitala and G. Ajmone Marsan (Springer, Cham, 2014), pp. 91–99.

[37] H. Freistühler and J. Fuhrmann, Nonlinear waves and polarization in diffusive directed particle flow, SIAM J. Appl. Math. **78**, 759 (2018).

[38] L. Girardin and D. Hilhorst, Spatial segregation limit of traveling wave solutions for a fully nonlinear strongly coupled competitive system, arXiv:2010.12205.

[39] P. Flynn, Q. Neville, and A. Scheel, Self-organized clusters in diffusive run-and-tumble processes, arXiv:1712.00112.

[40] E. P. Zemskov, M. A. Tsyganov, and W. Horsthemke, Oscillatory pulses and wave trains in a bistable reaction-diffusion system with cross diffusion, Phys. Rev. E **95**, 012203 (2017).

[41] E. P. Zemskov, M. A. Tsyganov, and W. Horsthemke, Oscillatory pulse-front waves in a reaction-diffusion system with cross diffusion, Phys. Rev. E **97**, 062206 (2018).

[42] E. P. Zemskov, M. A. Tsyganov, and W. Horsthemke, Oscillatory multipulsons: Dissipative soliton trains in bistable reaction-diffusion systems with cross diffusion of attractive-repulsive type, Phys. Rev. E **101**, 032208 (2020).

[43] H. P. McKean, Nagumo's equation, Adv. Math. **4**, 209 (1970).

[44] J. Rinzel and J. B. Keller, Traveling wave solutions of a nerve conduction equation, Biophys. J. **13**, 1313 (1973).

[45] J. Rinzel and D. Terman, Propagation phenomena in a bistable reaction-diffusion system, SIAM J. Appl. Math. **42**, 1111 (1982).

[46] V. Petrov, S. K. Scott, and K. Showalter, Excitability, wave reflection, and wave splitting in a cubic autocatalysis reaction-diffusion system, Philos. Trans. R. Soc. London **347**, 631 (1994).

[47] E. P. Zemskov, K. Kassner, and M. J. B. Hauser, Wavy fronts and speed bifurcation in excitable systems with cross diffusion, Phys. Rev. E **77**, 036219 (2008).